

# Surrogate Modeling for Explainable Predictive Time Series Corrections

Alfredo López\*      Florian Sobieczky\*

January 17, 2025

## Abstract

We introduce a local surrogate approach for explainable time-series analysis. An initially non-interpretable predictive model to improve the forecast of a classical time-series ‘base model’ is used. ‘Explainability’ of the correction is provided by fitting the base model again to the data from which the error prediction is removed (subtracted), yielding a difference in the model parameters which can be interpreted. We provide illustrative examples to demonstrate the potential of the method to discover and explain underlying patterns in the data.

## 1 Introduction

Explainable AI (XAI) is now a broad and eminent discipline and has seen a tremendous increase of demand, particularly for applications for which accountability of predictive models is crucial [18, 7, 4, 10]. In particular, AI in time series models needs explainable (i.e. interpretable [3]) results in data approximation and prognosis [24, 22, 37, 12]. Local surrogate modeling methods such as LIME [23, 17, 27, 30], SHAP [32, 9, 14] and others [5, 40] have delivered the possibility to interpret the action of predictive models around a specific instance, that is, in the *neighborhood* of a single data point in the input space. The local approach involves solving the problem of choosing the right size and position of the local subset in the incidence space where the surrogate is defined [33, 26, 41, 39, 19].

As model agnostic local surrogates are defined by the attempt to mimic any given black box *locally* by a different, interpretable model, uncertainties of these models may play a major role in the quality of the emergent explanations ([25], Sect. 5.1.11). From the viewpoint of defining explainability by local surrogates, it is therefore imperative to discuss *fidelity* (of the explaining model toward the one to be explained) in connection with model accuracy. Such a definition has been supplied in [31]. Similar to this work, we focus on explaining the action

---

\*Software Competence Center Hagenberg, Hagenberg, Austria

of a non-interpretable, high-performing predictive model in its role as a small *additive correction* to an interpretable base model (cf. [20]).

Further approaches yielding explanations of the action of predictive models can be seen in a particular branch of physics-informed, or knowledge-guided machine learning [29]. Also, entropy-based methods are successful in explaining time series anomalies in a physical context [2]. BAPC has a characteristic way of expressing explanations: To explain a single instance in the input space, a neighborhood is selected and another fit of the interpretable base model is carried out with data modified (corrected by the AI model to be explained) on just this neighborhood. The change of the interpretable fitting parameters is then taken as the 'explanation' of the local action of the correcting AI model (see Section 2).

The present work extends the BAPC method to time series modeling, where an interpretable time series model is combined with a correcting high performing machine learning model. The latter is explained inside a suitably chosen time window that assumes the role of the neighborhood. Instead of intervals or ball-shaped regions in  $\mathbb{R}^d$ , numbers of dimensions dating back in time from the current moment are considered, here (cf. 'window-length' in [40]).

Our main contribution consists in introducing the BAPC-approach [31, 20] to time series data. This refers to an additive *hybrid* model  $t \mapsto \hat{y}(t)$  consisting of an interpretable base model  $f_\theta(t)$ , explaining the bulk of the phenomenology of the series by interpretable fitted parameters, and an *AI-correction*  $\hat{\varepsilon}(t)$ , i.e., a machine learning model, predicting the residual error of the base model, however needing *interpretation*. This is delivered in the form of a local surrogate  $\Delta f_r = f_{\theta_0} - f_{\theta_r}$  given by the change  $\Delta\theta_r = \theta_0 - \theta_r$  of the base-model's parameters necessary to *locally* produce the observed correction within the fidelity-bounds without the help of the machine learning model. *Locally* means on a sub-window of size  $r$ .

We organize this paper as follows: In Section 2 theoretical setup for the concepts of BAPC for time series (SBAPC) is laid out. In Section 3 the connection between a physical and a time series model for discrete time is presented. Section 4 contains the description of another established concept from XAI (the integrated gradient method), and Section 5 contains the experiments - both, on artificial and real data.

## 2 BAPC

In this section, we specialize the "Before and After Prediction Parameter Comparison (BAPC)" framework proposed in [21] to the context of explainable time series forecasting. For a given real-valued time series  $y = (y_t)_{t=1}^n$  of finite length  $n \in \mathbb{N}$ , the BAPC consists of the following three steps:

**Step-1: First application of the base model.** Initially, the BAPC involves fitting a parametric *base model*  $f_\theta : \mathbb{R} \rightarrow \mathbb{R}$  on the time series  $y$ , resulting in

$$y_t = f_{\theta_0}(t) + \varepsilon_t, t = 1, \dots, n, \quad (1)$$

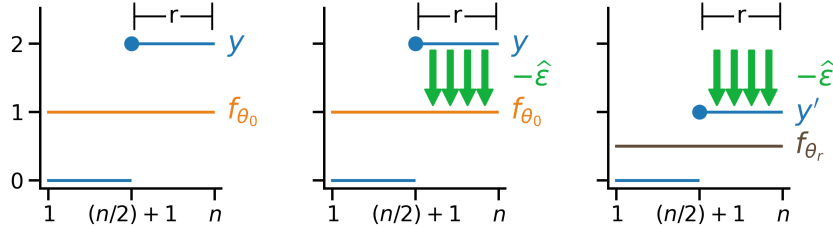
where  $\theta_0 = (\theta_{01}, \dots, \theta_{0q}) \in \mathbb{R}^q$  is the estimated parameter and  $\varepsilon_t := y_t - f_{\theta_0}(t)$ ,  $t = 1, \dots, n$ , are the residuals.

**Step-2: Application of the correction model.** The base model chosen in Step-1 is interpretable but lacks overall accuracy, which motivates the use of an additional correction. Therefore, in this step, we apply a *correction model*  $\hat{\varepsilon}$  to the residuals  $\varepsilon_1, \dots, \varepsilon_n$  obtained in Step-1, leading to the combined model  $f_{\theta_0} + \hat{\varepsilon}$ . The forecast generated by the combined model is expected to be accurate, but it will not be, in general, interpretable, prompting the subsequent step.

**Step-3: Second application of the base model.** In this step, we take a suitable *correction window size*  $r \in \mathbb{N}_0$  and compute the modified time series  $y' := (y'_t)_{t=1}^n$  defined as  $y'_t = y_t$  if  $1 \leq t \leq n - r$  and  $y'_t = y_t - \hat{\varepsilon}(t)$  if  $n - r < t \leq n$ . We then fit again the base model  $f_{\theta}$  to  $y'$  leading to estimated parameter  $\theta_r = (\theta_{r1}, \dots, \theta_{rq}) \in \mathbb{R}^q$ , the *BAPC-explanation*

$$\Delta\theta_r = (\Delta\theta_{r1}, \dots, \Delta\theta_{rq}) := \theta_0 - \theta_r \in \mathbb{R}^q \quad (2)$$

and the *surrogate model*  $f_r := f_{\theta_0} + \Delta f_r$ , where  $\Delta f_r := f_{\theta_0} - f_{\theta_r}$  is the *surrogate correction*. Figure 1 illustrates the BAPC applied to a constant piecewise time series.



**Step-1:** First application of the base model. **Step-2:** Application of the correction model. **Step-3:** Second application of the base model.

Figure 1: The BAPC approach is applied to a piecewise constant time series  $y$  of even length  $n$  and a "jump" (step) of size 2 at  $(n/2) + 1$ . Initially, in Step-1, a constant function  $f_{\theta}(t) = \theta$  is used as the base model, leading to  $\theta_0 = 1$ . In Step-2, the 1-nearest-neighbor interpolation  $\hat{\varepsilon}$  (represented by the arrows), is applied. During Step-3, using a window size  $r = n/2$ , the modified time series  $y'$  has a jump of size 1 at  $(n/2) + 1$ . Consequently, the corrected parameter becomes  $\theta_r = 0.5$ , providing an explanation  $\Delta\theta_r = \theta_0 - \theta_r = 1 - 0.5 = 0.5$ , which points in the (upward) direction of  $\hat{\varepsilon}$  within the correction window. See Fig. 3a for the resulting surrogate (orange).

For the observations  $y_1, y_2, \dots, y_m$  of a time series taking place consecutively over time, it is of interest to apply the BAPC sequentially for each point in time using the most recent data of a sliding window. We define sequential BAPC (SBAPC) as the process of consecutively applying BAPC to  $y_{s-n+1}, \dots, y_s$ , for every  $s = n, \dots, m$ , where  $1 \leq n \leq m$  is a fixed training set size. The BAPC-

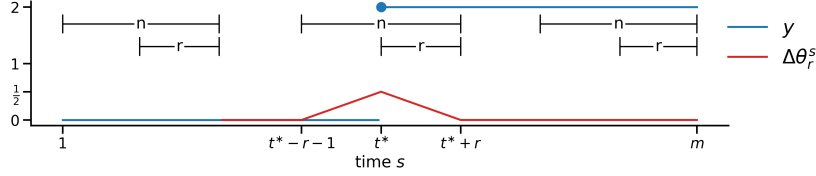


Figure 2: The sequential-BAPC is applied to a piecewise constant step function (blue) having a discontinuity at time  $t^*$ , in a similar setting as in Figure 1, using the constant function as the base model, 1-nearest-neighborhood interpolation as the correction model, and a correction window size  $r = n/2$  with even  $n$ . The operation on the sliding window with end-points  $s - n$  and  $s$ , for  $s = n, \dots, m$  (horizontal bracketed lines), leads to the SBAPC-explanation  $\Delta\theta_r^s$  (red).

explanation at time  $s$  is given by

$$\Delta\theta_r^s := (\Delta\theta_{r1}^s, \dots, \Delta\theta_{rq}^s) = \theta_0^s - \theta_r^s \in \mathbb{R}^q \quad (3)$$

where  $\theta_0^s = (\theta_{01}^s, \dots, \theta_{0q}^s)$  and  $\theta_r^s = (\theta_{r1}^s, \dots, \theta_{rq}^s)$  are the parameters obtained, respectively, after Step-1 and Step-3 of BAPC applied to  $y_{s-n+1}, \dots, y_s$ . The surrogate model at time  $s$  is  $f_r^s := f_{\theta_0^s} + \Delta f_r^s$ , where  $\Delta f_r^s := f_{\theta_0^s} - f_{\theta_r^s}$  is the surrogate correction at time  $s$ . The SBAPC employs a sliding window approach, wherein an  $n$ -size training window is moved step by step across the dataset to derive explainability from local sections of the time series. The correction window is defined as the most recent  $r$  points within the training window. The SBAPC is illustrated in Figure 2.

### 3 Base model

As a base model, we use a function describing decaying oscillations

$$f_{\theta}(t) = \alpha \exp(-\beta t) \cos(\omega t + \phi), \quad (4)$$

with  $\theta = (\alpha, \beta, \omega, \phi)$ ,  $\alpha, \omega \in \mathbb{R}_+$ ,  $\beta \in \mathbb{R}$  and  $\phi \in [0, 2\pi]$ , representing amplitude, logarithmic decrement, frequency, and phaseshift, respectively. The function (4) is the solution of the simple harmonic oscillator [6], a model that plays an important role in time series analysis, particularly in understanding periodic behavior, modeling oscillations, and analyzing dynamical systems. Another related formulation that we consider in this paper is the deterministic autoregressive sequence AR(2), which is a particular case of the widely used ARIMA models [16]. We say that  $y = (y_t)_{t=1}^n$  is a AR(2) sequence with coefficients  $\varphi_1, \varphi_2 \in \mathbb{R}$  if

$$y_t = \varphi_1 y_{t-1} + \varphi_2 y_{t-2}, \quad t = 3, \dots, n. \quad (5)$$

Observe that models (4) and (5) are fully characterized by  $(\alpha, \beta, \omega, \phi)$  and  $(y_1, y_2, \varphi_1, \varphi_2)$  respectively. The following two propositions show the connection between these two models; the proofs are postponed to the Appendix A.1.

**Proposition 1.** Let  $y_t = \alpha \exp(-\beta(t-1)) \cos(\omega(t-1) + \phi)$  for  $t = 1, \dots, n$ , with  $\alpha, \omega \in \mathbb{R}_+$ ,  $\beta \in \mathbb{R}$  and  $\phi \in [0, 2\pi]$ . Then  $(y_t)_{t=1}^n$  is a AR(2) sequence with  $y_1 = \alpha \cos(\phi)$ ,  $y_2 = \alpha \exp(-\beta) \cos(\omega + \phi)$ ,  $\varphi_1 = 2 \exp(-\beta) \cos(\omega)$  and  $\varphi_2 = -\exp(-2\beta)$ .

**Proposition 2.** Let  $(y_t)_{t=1}^n$  be a AR(2) sequence with coefficients  $\varphi_1 \in \mathbb{R}$ ,  $\varphi_2 < 0$ , then  $y_t = \alpha \exp(-\beta(t-1)) \cos(\omega(t-1) + \phi)$  for  $t = 1, \dots, n$ , with  $\beta = -\frac{1}{2} \ln(-\varphi_2)$ ,  $\omega = \arccos(\frac{1}{2}\varphi_1 \exp(\beta))$ ,  $\phi = \text{atan}\left(\frac{y_1 \exp(-\beta) \cos \omega - y_2}{y_1 \exp(-\beta) \sin \omega}\right)$  and  $\alpha = y_1 \sqrt{1 + \tan^2 \phi}$ .

Being able to switch between (4) and (5) allows obtaining physical interpretations of discrete time series data specific to explanations in the sense of SBAPC. The following statement provides a characterization of the AR(2) process dynamic in dependence of the initial conditions that is explicit in time and in the auto-regressive coefficients.

**Proposition 3.** Let  $(y_t)_{t=1}^n$  be an AR(2) sequence with coefficients  $\varphi = (\varphi_1, \varphi_2)$ . Then

$$y_t = \Phi_1(t, \varphi)y_2 + \Phi_2(t, \varphi)y_1, \quad t = 1, \dots, n,$$

where  $\Phi_1(1, \varphi) = 0$ ,  $\Phi_1(2, \varphi) = 1$ ,  $\Phi_1(t, \varphi) = \Phi_1(t-2, \varphi)$ ,  $\Phi_2(1, \varphi) = 1$ ,  $\Phi_2(2, \varphi) = 0$ ,  $\Phi_2(t, \varphi) = \varphi_2 \Phi_2(t-3, \varphi)$ , for  $t = 3, \dots, n$ , and

$$\Phi(t, \varphi) = \sum_{k=0}^{\lfloor t/2 \rfloor} \binom{t-k}{k} \varphi_1^{t-2k} \varphi_2^k, \quad t = 3, \dots, n. \quad (6)$$

*Proof.* Let us denote  $z_t = \begin{pmatrix} y_{t+1} \\ y_t \end{pmatrix}$ ,  $A = \begin{pmatrix} \varphi_1 & \varphi_2 \\ 1 & 0 \end{pmatrix}$  and  $A^t = \begin{pmatrix} a^{(t)} & b^{(t)} \\ c^{(t)} & d^{(t)} \end{pmatrix}$ . From the state space representation  $z_t = Az_{t-1}$  we obtain  $z_t = A^{t-1}z_1$  and so

$$y_t = a^{(t-1)}y_2 + b^{(t-1)}y_1, \quad t = 3, \dots, n. \quad (7)$$

Then the result follows from (7) and Theorem 1 in [13].  $\square$

## 4 Explanation importance

The SBAPC explanation,  $\Delta\theta_r$ , defined in Section 2, is a vector of parameter changes of which each coordinate is designed to capture the respective feature's influence on the correction model's predictions. In this section, we introduce the SBAPC Integrated Gradient Score, an adaptation of the Integrated Gradients method [34, 15], which aims to quantify and compare the importance of these explanations. Throughout this discussion, we retain the notation and definitions established in Sections 2 and 3. We assume that the mapping  $\theta \mapsto f_\theta(t)$  is differentiable for every  $t \in \mathbb{R}$ , and we denote the partial derivative of  $\theta \mapsto f_\theta(t)$  with respect to  $\theta_k$  at  $\theta' \in \mathbb{R}^q$  by  $\frac{\partial f}{\partial \theta_k}(t, \theta')$ .

**Definition 1.** The segment joining  $\mathbf{a} \in \mathbb{R}^n$  and  $\mathbf{b} \in \mathbb{R}^n$  is defined by the function  $\gamma : \mathbb{R}^{2n} \times [0, 1] \rightarrow \mathbb{R}^n$ ,  $h \mapsto \gamma(\mathbf{a}, \mathbf{b}, h) := \mathbf{a} + h(\mathbf{b} - \mathbf{a})$ .

**Definition 2.** The BAPC integrated gradient of the  $k$ -th explanation at  $t \in \mathbb{R}$  is defined as

$$\text{IG}_k(f_\theta, t) := \Delta\theta_{rk} \int_0^1 \frac{\partial f}{\partial \theta_k}(t, \gamma(\boldsymbol{\theta}_r, \boldsymbol{\theta}_0, h)) dh. \quad (8)$$

For the sequential setting with  $m$  observations, we define the SBAPC integrated gradient of the  $k$ -th explanation at  $s \in \{n, \dots, m\}$  and  $t \in \mathbb{R}$  as

$$\text{IG}_k(f_\theta, s, t) := \Delta\theta_{rk}^s \int_0^1 \frac{\partial f}{\partial \theta_k}(t, \gamma(\boldsymbol{\theta}_r^s, \boldsymbol{\theta}_0^s, h)) dh. \quad (9)$$

We will also denote  $\text{IG}(f_\theta, s) := (\text{IG}_1(f_\theta, t), \dots, \text{IG}_1(f_\theta, q))$  and  $\text{IG}(f_\theta, s, t) = (\text{IG}_1(f_\theta, s, t), \dots, \text{IG}_q(f_\theta, s, t))$ .

**Observation 1.** In the sequential setting,  $\text{IG}(f_\theta, s, t)$  corresponds to the importance of past predictions, current point in time prediction or future forecast depending on whether  $t < s$ ,  $t = s$  or  $t > s$  respectively.

The following result is a direct consequence of the completeness of Integrated Gradients.

**Proposition 4.** The sum of the BAPC integrated gradients components is equal to the correction surrogate, namely

$$\sum_{k=1}^q \text{IG}_k(f_\theta, t) = \Delta f_r(t). \quad (10)$$

*Proof.* The result follows directly from Proposition 1 in [34] and the Fundamental Theorem of Calculus.  $\square$

We now derive  $\text{IG}(f_\theta, t)$  formulas for the case of a linear base model and for the base models considered in Section 3.

**Proposition 5.** For any  $t \in \mathbb{R}$ , we have the following.

1. If  $f_\theta(t) = \boldsymbol{\theta}^\top g(t)$  with  $\boldsymbol{\theta} \in \mathbb{R}^q$  and  $g(t) = (g_1(t), \dots, g_q(t))$  then

$$\text{IG}_k(f_\theta, t) = \Delta\boldsymbol{\theta}_{rk} g(t), \quad k = 1, \dots, q.$$

2. If  $f_\theta(t) = \alpha \exp(-\beta t) \cos(\omega t + \phi)$ , with  $\boldsymbol{\theta} = (\alpha, \beta, \omega, \phi)$ , then

$$\text{IG}(f_\theta, t) = \text{Re} \left( \begin{array}{c} \Delta\alpha_r \Delta g_r(t) \\ \frac{-\Delta\beta_r t}{-\Delta\beta_r t + i\Delta\omega_r t + i\Delta\phi_r} (\Delta f_r(t) - \Delta\alpha_r \Delta g_r(t)) \\ \frac{i\Delta\omega_r t}{-\Delta\beta_r t + i\Delta\omega_r t + i\Delta\phi_r} (\Delta f_r(t) - \Delta\alpha_r \Delta g_r(t)) \\ \frac{i\Delta\phi_r}{-\Delta\beta_r t + i\Delta\omega_r t + i\Delta\phi_r} (\Delta f_r(t) - \Delta\alpha_r \Delta g_r(t)) \end{array} \right) \quad (11)$$

where

$$\Delta g_r(t) := \frac{\exp(-\beta_0 t + i\omega_0 t + i\phi_0) - \exp(-\beta_r t + i\omega_r t + i\phi_r)}{-\Delta\beta_r t + i\Delta\omega_r t + i\Delta\phi_r}.$$

3. If  $f_\theta(t) = \Phi_1(t, \varphi)y_2 + \Phi_2(t, \varphi)y_1$  with  $\theta = \varphi = (\varphi_1, \varphi_2)$  and  $\Phi_1, \Phi_2$  defined in Proposition 3, then  $\text{IG}_1(f_\theta, 0) = \text{IG}_1(f_\theta, 1) = \text{IG}_2(f_\theta, 0) = \text{IG}_2(f_\theta, 1) = 0$  and, for  $t = 3, \dots, n$ , it hold that

$$\text{IG}_1(f_\theta, t) = \bar{\Phi}_1(t-2, 0)y_2 + \bar{\Phi}_1(t-3, 1)y_1 \quad (12)$$

$$\text{IG}_2(f_\theta, t) = \bar{\Phi}_2(t-2, 0)y_2 + \bar{\Phi}_2(t-3, 1)y_1, \quad (13)$$

where

$$\bar{\Phi}_1(t, j) = \Delta\varphi_{r1} \sum_{k=0}^{\lfloor t/2 \rfloor} \binom{t-k}{k} (t-2k) \Gamma_{k+j}^{t-1-2k},$$

$$\bar{\Phi}_2(t, j) = \Delta\varphi_{r2} \sum_{k=0}^{\lfloor t/2 \rfloor} \binom{t-k}{k} (k+j) \Gamma_{k-1+j}^{t-2k}$$

$$\text{and } \Gamma_n^m = \sum_{j=0}^m \sum_{k=0}^n \binom{m}{j} \binom{n}{k} (j+k+1)^{-1} \varphi_{r1}^{m-j} \Delta\varphi_{r1}^j \varphi_{r2}^{n-k} \Delta\varphi_{r2}^k.$$

*Proof.*

1. For any  $\theta' \in \mathbb{R}^q$  we have  $\frac{\partial f}{\partial \theta_k}(t, \theta') = g_k(t)$  and therefore  $\text{IG}_k(f_\theta, t) = \Delta\theta_{rk} \int_0^1 g_k(t) dh = \Delta\theta_{rk} g_k(t)$ .
2. The result follows from Lemma 1, after projecting (16) and (17) onto the real coordinate and taking  $x = \alpha_r$ ,  $\Delta x = \Delta\alpha_r$ ,  $y = (\beta_r, \omega_r, \phi_r)$ ,  $\Delta y = (\Delta\beta_r, \Delta\omega_r, \Delta\phi_r)$  and  $\mu = (-t, it, i)$ .
3. The formula follows after manipulating (6); see the Appendix A.1 for the proof. □

## 5 Experiment and analysis

In this section, we demonstrate and evaluate the proposed method using four synthetic and one real-world time series datasets, proceeding in increasing order of complexity<sup>1</sup>.

### 5.1 Trend change point

The first row in Figure 3 displays three synthetic time series corresponding to (a) step, (b) ramp, and (c) sinusoidal patterns. In Appendix A.2 we show that these data correspond to discrete observations from one dimensional dynamical systems governed by a non-homogeneous ODE. Each of these time series has a length of  $n = 96$  and a change point at  $t = 49$ , associated respectively with (a) intercept, (b) intercept and slope, and (c) amplitude and phase. For each

<sup>1</sup>Numerical implementation at <https://github.com/alflopezalfa/pitsa.git>

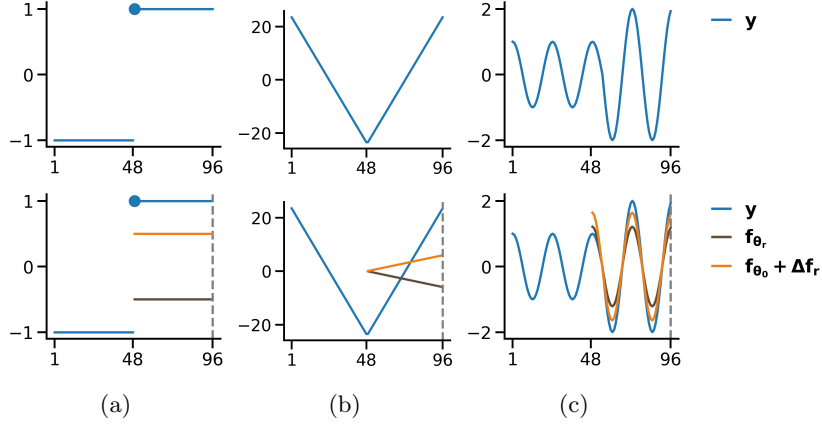


Figure 3: Experimental evaluation on (a) step, (b) ramp and (c) sinusoidal data. Each time series has length  $n = 96$  and a change point at  $t = 49$  associated to (a) intercept, (b) intercept and slope and (c) amplitude and phase. The surrogate of the hybrid model is shown by the orange curves: For (a), an increase in the intercept, for (b) an increase in the slope together with a decrease in the intercept, and for (c) a growing in amplitude with a small phase adjustment.

of these input time series, we carry out BAPC with a correction window size of  $r = 40$  and the base model  $f_\theta$  described in the third column of Table 1. For correction model we take the 1-Nearest-Neighbors regression, which is well suited for the current illustrative example as generate perfect fit on train data. On the other hand, the 1-Nearest-Neighbors is very prone to overfitting, hence in oncoming examples we will consider an actual AI model option. The second row in Figure 3 shows the base model after correction (brown line  $f_{\theta_r}$ ) and the surrogate model (orange line  $f_\theta + \Delta f_r$ ). As expected, the surrogate model aligns with the direction of the change in the data within the correction window relative to the remaining training window.

From Proposition 5-(1)-(2), we obtain the expression for  $IG(f_\theta, t)$  shown at the fourth column of Table 1, where  $\Delta g_r(t) = \sin(\omega t + \phi_0) - \sin(\omega t + \phi_r)$ . The last two columns show the explanation  $\Delta \theta_r$  and integrated gradient  $IG(f_\theta, t)$  at  $t = 96$ . From these values, we conclude that the method effectively explain the correction model prediction and generates a meaningful feature importance ranking of these explanations in terms of the base model parameters.

Table 1: Experimental configuration and results for step, ramp and sinusoidal with amplitude change point (SinACP) data.

Data	$\theta$	$f_\theta(t)$	$IG(f_\theta, t)$	$\Delta \theta_r$	$IG(f_\theta, t = 96)$
Step	$a$	$a$	$\Delta a_r$	0.5	0.5
Ramp	$(a, b)$	$a + bt$	$(\Delta a_r, \Delta b_r t)$	(-6, 0.1)	(-6, 12)
SinACP	$(\alpha, \phi)$	$\alpha \cos(2\pi t + \phi)$	$(\Delta \alpha_r \Delta g_r(t), \Delta f_r(t) - \Delta \alpha_r \Delta g_r(t))$	(0.2, 0.01)	(0.2, 0.004)



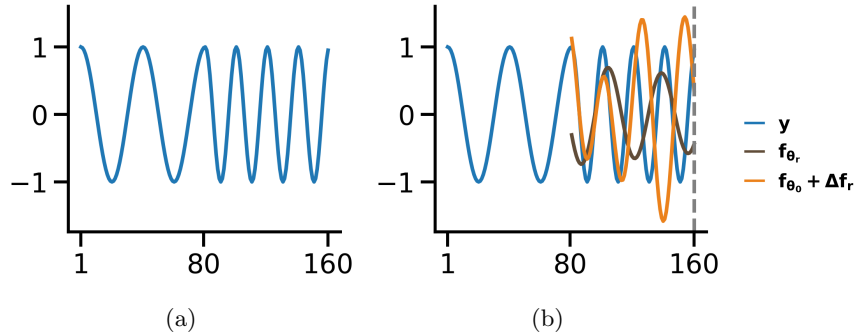


Figure 4: Experimental evaluation on synthetic time-series with frequency and phase change point.

## 5.2 Frequency change point

We now apply the proposed method to the more challenging case of a sinusoidal time series of length  $n = 160$ , featuring a frequency and phase change point at  $t = 81$ ; see Figure 4a. This time series corresponds to discrete observations derived from a linear ODE with time-dependent coefficients; see Appendix A.2. The sequential BAPC is applied taking a correction window size of  $r = 80$  and the 1-Nearest-Neighbor correction model. We use the AR formulation (5) as the base model, where the parameters  $\varphi = (\varphi_1, \varphi_2)$  are estimated via *robust* auto-regression.

Robust AR on a time series  $(z_t)_{t=1}^n$  involves first removing outliers from the set  $\{x_t\}_{t=3}^n := \{(z_{t-1}, z_{t-2})\}_{t=3}^n$  and then performing linear regression of  $\{z_t\}_{t \in I}$  against  $\{x_t\}_{t \in I}$ , where  $I$  is the set of indices after outlier removal. The time series in Figure 4a exhibits no discontinuities; hence, no outliers are removed during the first application of the robust AR base model. On the other hand, applying robust AR after correction, removes the outlier  $x_{82} = (y'_{81}, y'_{80}) = (y_{81} - \hat{\varepsilon}_{81}, y_{80})$ , thereby alleviating the model misspecification induced by the discontinuity in  $y'$  at  $t = 81$ . Figure 4b shows the base model after correction (brown line  $f_{\theta_r}$ ) and the surrogate model (orange line  $f_{\theta_0} + \Delta f_r$ ).

The first row in Table 2 shows the BAPC configuration and results at  $t = 160$ , where, in particular, the explanation and integrated gradient were computed from the formula at Proposition 5-3. Interpreting these results is not straightforward; hence, we make use of Proposition 2 to analyze the BAPC results in the context of the sinusoidal base model  $f_{\theta}(t) = \alpha \exp(-\beta t) \cos(\omega t + \varphi)$ , with  $\theta = (\alpha, \beta, \omega, \varphi)$ . From Proposition 5-2, we obtain the integrated gradient  $\text{IG}(f_{\theta}, t = 160)$  value shown in the second row of Table 2. This value identifies a significant increase in frequency and a minor adjustment in phase, both of which are present in the input data and captured by the 1-Nearest-Neighbor correction. Additionally, it indicates a small change in the exponential decay parameter, which is absent in the data. Such inaccuracy could potentially be mitigated by increasing the sampling frequency, at the expense of the high floating-point

precision required to compute the combinatorial formulas (12) and (13).

Table 2: Experimental configuration and results for sinusoidal data with frequency change point (SinFCP).

Data	$\theta$	$f_\theta(t)$	$\text{IG}(f_\theta, t)$	$\Delta\theta_r \times 1e2$	$\text{IG}(f_\theta, t = 160) \times 1e2$
SinFCP	$(\varphi_1, \varphi_2)$	Eq. (5)	Eq. (12), (13)	(-3.1, 0.3)	(46, -6)
	$(\alpha, \beta, \omega, \phi)$	$\alpha \exp(-\beta t) \cos(\omega t + \phi)$	Eq. (11)	(0.4, 0.2, 6.6, -5.2)	(0.0, -1.9, 41.7, -0.2)

While it might seem reasonable to use  $f_{(\alpha, \beta, \omega, \phi)} = \alpha \exp(-\beta t) \cos(\omega t + \varphi)$  directly instead of the AR formulation, this approach is not well-suited for the current example. Indeed, it can be shown that  $\omega \mapsto \sum_{t=1}^n (y_t - f_{(\alpha, \beta, \omega, \phi)}(t))^2$  has two global minima, attained at the data frequency values before and after the change point. As a result, in this example, this would lead to  $\Delta\omega_r = 0$ .

Finally, observe that if the base model  $f_\theta$  is linear with respect to  $\theta$ , then the surrogate model belongs to the same model class. More specifically, in this case,  $f_{\theta_0} + \Delta f_r = f_{\theta_0 + \Delta\theta_r}$ , as in Figure 3a and Figure 3b. Note also that  $f_{\theta_0} + \Delta f_r \approx f_{\theta_0 + \Delta\theta_r}$  for the scenario depicted in Figure 3c, where equality would hold if  $\Delta\phi_r = 0$ . In general, for the non-linear case, the surrogate model  $f_{\theta_0} + \Delta f_r$  does not belong to the same class as the base model, as shown in Figure 4b, where  $f_{\theta_0} + \Delta f_r$  has non constant amplitude.

### 5.3 Trend change point with varying correction window size

In this section, we investigate the impact of the correction window size on the BAPC and provide insights into its optimal selection. The step and ramp time series introduced in Section 5.1, depicted in figures 5a and 6a, respectively, are used as input data. For this experiment, we employ the base models specified in Table 1, with the correction model implemented as an LSTM recurrent neural network [11]. This widely used time-series forecasting model is known for its ability to capture complex data patterns without requiring explicit assumptions about the underlying system’s mathematics or physics. We choose an auto-regressive order  $p = 12$  which provides a trade-off between lagged dependency and the train set size at each time step  $s$ . We then compute the BAPC by varying the window size across a range of values,  $r = 0, \dots, n$ .

To determine the optimal window size at a given time  $t$ , we propose using  $r \mapsto |\Delta f_r^s(t)|$  as the objective function. Using this criterion, the optimal window size is found to be  $r = 48$  and  $r = 24$  for the step and ramp input data, respectively, as illustrated in figures 5b and 6b. Our results suggest that the optimal window size depends on the type of change-point or anomaly in the data, as well as the AI-correction framework and the choice of the base model. Future research will further explore this dependency and refine the proposed approach.

It is also of interest to compare our approach to other explainable time-series methods. LIME [23] is an explainable AI framework designed to provide locally interpretable explanations for complex machine learning models. In the context

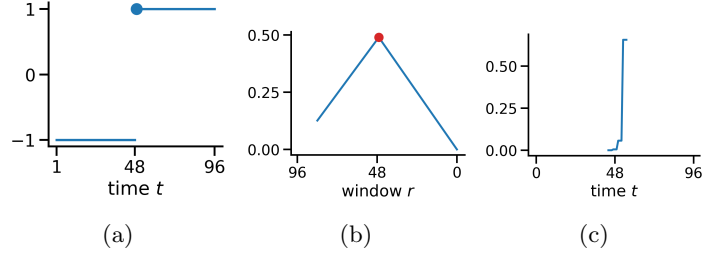


Figure 5: Experimental evaluation of BAPC for different window sizes over the step input data (a). The surrogate correction  $r \mapsto \Delta f_r(t)$  at  $t = 96$  (b), attains a global maximum at  $r = 48$ . The LIME (c) also provides information on the change point location.

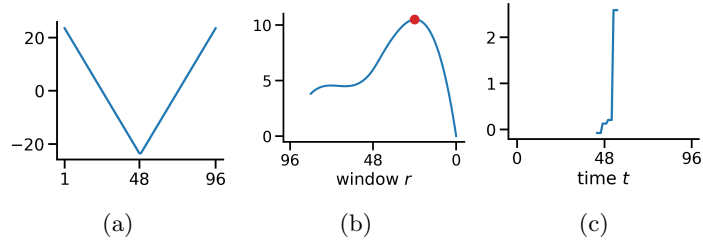


Figure 6: Experimental evaluation of BAPC for different window sizes over the ramp input data (a). The surrogate correction  $r \mapsto \Delta f_r(t)$  at  $t = 96$  (b), attains a global maximum at  $r = 24$ . The LIME (c) also provides information on the change point location.

of time series and auto-regressive models, LIME can be used to understand the impact of individual time steps or features on the model’s predictions [28]. The process involves perturbing the input data, generating predictions, and fitting a local interpretable model.

Let us briefly describe the application of LIME in the context of this paper. For a residual time series  $(\varepsilon_t)_{t=1}^n$  and a (previously fit) correction model  $\widehat{\varepsilon}$  of auto-regressive order  $p$ , we define  $\{x_t\}_{t=p+1}^n := \{(\varepsilon_{t-1}, \dots, \varepsilon_{t-p})\}_{t=p+1}^n$ . Given an instance  $x_t$ , the goal of LIME is to explain the black-box prediction  $\widehat{\varepsilon}(x_t)$  in terms of individual coordinates of  $x_t$ . To achieve this, a partition of  $x_t$  consisting of contiguous segments of suitable sizes, is computed. A new set of  $k$  perturbed samples  $x'_1, \dots, x'_k$  is then generated by randomly selecting segments of the partition and replacing the values in these segments with a non-informative placeholder. Next, a linear regression of the predictions  $y'_1, \dots, y'_k$  against the perturbed samples  $x'_1, \dots, x'_k$  is performed, where  $y'_1 := \widehat{\varepsilon}(x'_1), \dots, y'_k := \widehat{\varepsilon}(x'_k)$ . Finally, the resulting vector  $c_t$  of  $p$  coefficients from the regression is interpreted as a measure of how each input data point  $(\varepsilon_{t-1}, \dots, \varepsilon_{t-p})$  contributes to the prediction  $\widehat{\varepsilon}_t := \widehat{\varepsilon}(\varepsilon_{t-1}, \dots, \varepsilon_{t-p})$ .

We applied LIME to the residuals and the correction model obtained after

Step-2 of the BAPC, resulting in coefficients  $c_t = (c_{t1}, \dots, c_{tp})$  for  $t = p + 1, \dots, n$ . Figures 5c and 6c display  $c_t$  plotted against  $t - p, \dots, t - 1$  for  $t = 56$ , corresponding to the step and ramp data, respectively. The time point  $t = 56$  was chosen for visualization due to its proximity to the change point. A change in the coefficient patterns associated with the change point is observed, aligning with the findings from BAPC. We suggest that BAPC and LIME have the potential to provide valuable complementary insights, subject to further adaptations.

#### 5.4 Trend change point on sequential setting

Let us now apply the sequential BAPC to the step time series  $(y_s)_{s=1}^m$  of length  $m = 240$ , shown in Figure 7a. For each  $s = n, \dots, m$ , we apply BAPC to the segment  $(y_t)_{t=s-n+1}^s$  with  $n = 96$ ,  $r = 48$ , and the base model  $f_\theta(t) = \alpha$ , where  $\theta = \alpha$ . For the correction model, we utilize an LSTM recurrent neural network with auto-regressive order  $p = 12$ . We also applied the sequential BAPC to the ramp data shown in Figure 7b under the same setting described before, but taking the base model  $f_\theta(t) = \alpha + \beta t$ , where  $\theta = (\alpha, \beta)$ .

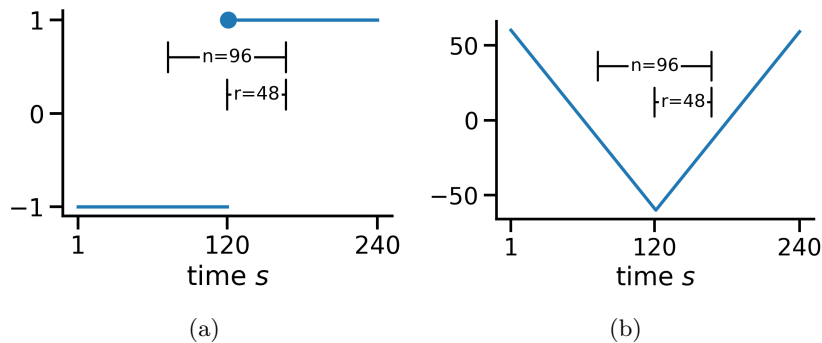


Figure 7: Input step (a) and ramp (b) time series for the sequential BAPC. The horizontal bracketed lines depict the sliding window centered at the change point.

Observe that from Proposition 4, we have

$$\sum_{k=1}^q \text{IG}_k(f_\theta, s, t) = \Delta f_r^s(t), \quad (14)$$

which justify the use of  $(s, t) \mapsto \Delta f_r^s(t)$  as an overall score to assess changes in the BAPC outcome over time. In this context, we aim to investigate the local maxima and minima of the mapping  $(s, t) \mapsto \Delta f_r^s(t)$  to understand the behavior of the underlying AI correction. To this end, let us examine the heatmaps of  $\Delta f_r^s(t)$  for  $s = n, \dots, m$  and  $t = s - n + 1, \dots, s$ , displayed in Figure 8 for the case of the (a) step and (b) ramp data.

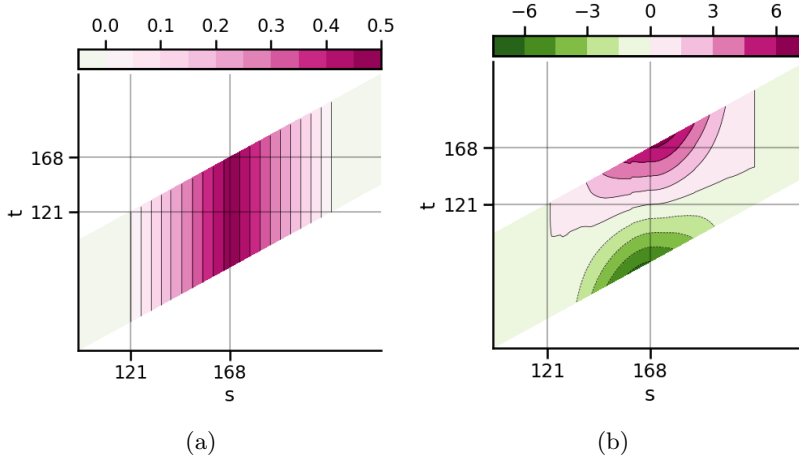


Figure 8: Sequential BAPC results: For the step (a) and ramp (b) data, the surrogate correction  $(s, t) \mapsto \Delta f_r^s(t)$  attains (non-unique) extreme values when  $s = 168$ , which corresponds to the training window of size  $n$  being centered at the change point; see Figure 7.

From Figure 8a, we observe that for the step data case, the surrogate correction  $(s, t) \mapsto \Delta f_r^s(t)$  attains a global maximum at  $s = 168$  and for every  $t$  in the associated training window,  $t = s - n, \dots, s$ . For the ramp data case, shown in Figure 8b, the surrogate correction  $(s, t) \mapsto \Delta f_r^s(t)$  reaches a global minimum at the left endpoint of the correction window ( $t = s - n$ ) and a global maximum at the right endpoint ( $t = s$ ). The situation  $s = 168$  corresponds to the training window being centered at the change point, as depicted in Figure 7. These observations suggest that the local maxima and minima of  $(s, t) \mapsto \Delta f_r^s(t)$  are associated with change points in the data, provided they are captured by the AI corrections. A detailed investigation of these optimal points and their relationship with  $n$  and  $r$  lies beyond the scope of this paper and will be addressed in future research.

## 5.5 Air passenger dataset

We continue the experimental validation by applying the proposed method to the air-passenger dataset [35], a well-known dataset commonly used in time series analysis and machine learning studies. This dataset contains  $m = 144$  monthly totals of international airline passengers (in thousands) from January 1949 to December 1960. For this experiment, we aim to analyze how passenger demand evolves over time on an annual basis, with a specific focus on the last four years of the dataset.

To achieve this, we compute the sequential BAPC with a training window

size of  $n = 48$ , a correction window size of  $r = 12$ , base model

$$f_{\theta}(t) = a + bt + ct^2 + \alpha \cos\left(\frac{2\pi}{12}t + \phi\right), \quad (15)$$

where  $\theta = (a, b, c, \alpha, \phi)$  represents the intercept, slope, quadratic term, amplitude, and phase. This model combines a polynomial trend with a periodic pattern. The LSTM recurrent neural network of auto-regressive order  $p = 12$  is used as the correction model.

The surrogate correction  $(s, t) \mapsto \Delta f_r^s(t)$  is shown in Figure 10a. From the figure, we observe that the surrogate correction attains its minimum and maximum values for  $s = 1960$ . In other words, there is not only a noticeable increase in the general trend of the data, as apparent from Figure 10, but also an increase in the complexity of the corrections applied on top of that trend, as modeled by the black-box LSTM. The surrogate correction quantifies the magnitude of the AI correction.

To enhance explainability, we utilize Proposition 4 and Proposition 5 to decompose the surrogate correction  $(s, t) \mapsto \Delta f_r^s(t)$  (Figure 10a) into its integrated gradient components  $(s, t) \mapsto \text{IG}_k(f_{\theta}, s, t)$  associated with the base model parameters: the intercept  $a$ , slope  $b$ , quadratic term  $c$ , amplitude  $\alpha$ , and phase  $\phi$ . From these figures, we observe that most of the surrogate correction is attributed to the polynomial trend. However, it is also noteworthy that the amplitude integrated gradient reveals interesting patterns, while the phase integrated gradient suggests that the corrections maintain a degree of continuity.

In conclusion, the BAPC framework delivers explainability for the black-box correction model (in this case, the LSTM) by framing it within the structure of the chosen base model. We believe that, in applications requiring explainability, additional expert knowledge is crucial for configuring the method (e.g., selecting the training window, correction window, base model, and correction model) and interpreting the results of the proposed approach.

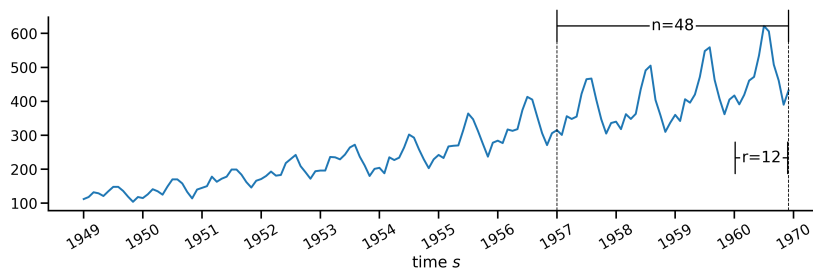


Figure 9: Air passenger time series.

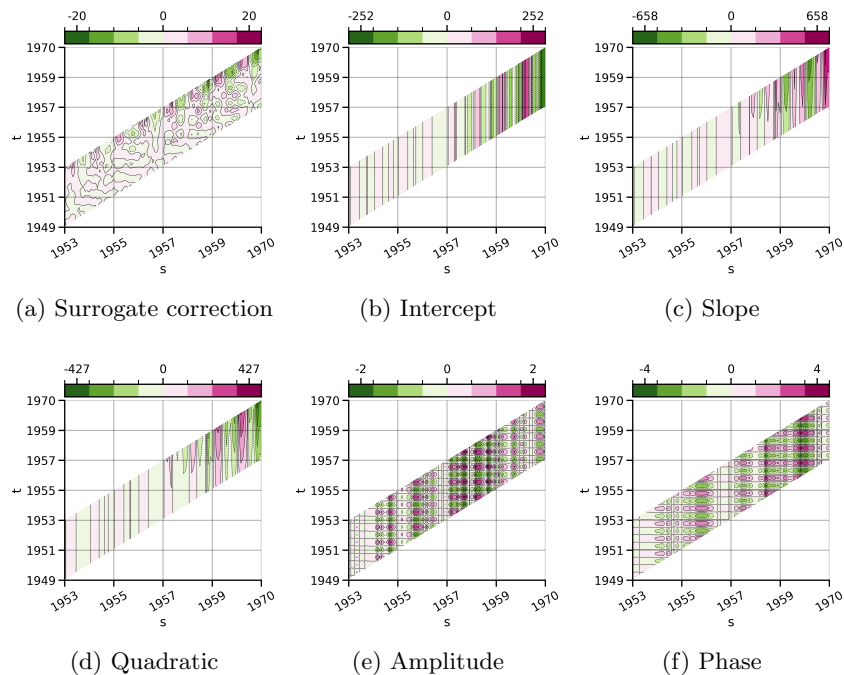


Figure 10: Sequential BAPC on air-passenger data. The heatmaps corresponds to (a) surrogate correction  $(s, t) \mapsto \Delta f_r^s(t)$  and the integrated gradient  $(s, t) \mapsto \text{IG}_k(f_\theta, s, t)$  associated to the intercept  $a$ , slope  $b$ , quadratic term  $c$ , amplitude  $\alpha$ , and phase  $\phi$ : The strong coloring show the intervals of the features being particularly significant for the correction  $\hat{\epsilon}$  (e.g., the importance of an upward directed quadratic term after 1959, well visible in Fig. 9).

## 6 Conclusions

We defined an extension of the BAPC method for time series based on the notion of being able to compare the change in the model parameters of an interpretable time series model before and after the application of a complex black box correction model. In particular, we defined the concept of sequential BAPC leading to an explainable time series model for each point in time, by means of a time dependent explanation.

The optimal choice of the correction window (locality problem in local surrogate modeling; see Question 3 in [26]) is our primary focus of ongoing research, which we plan to propose in the form of a sequential BAPC with adaptive correction window value. The presented illustrative example provides initial insights, by linking the explanation with the discovery and explanation of change points in the data.

It is seen that BAPC is able to deliver explanations of changes in a sequence of observations by changes of parameters associated with a law of motion if taken

as a physical model for observed time series data, linking it to physics informed machine learning [29]. Furthermore, it is able to distinguish the parameters most responsible for this change from others, delivering 'feature-importance' [4] in the sense of local surrogate modeling in explainable AI. Moreover, we also see that knowledge of the underlying physics flow in two directions: initial knowledge of the physics is used in the form of the base model (a sinusoidal function) and then the method delivers back further explanations of the system dynamics (the presence of an amplitude and phase change point). As such the proposed method goes beyond mere data driven explainability, but provides interpretations of predictive models in terms of physical views set up by the choice of the base model [1]. In this context, we are currently working on extending the results in Section 3 by establishing the connection between auto-regressive models of general order and ODE solutions. Such a framework would enable the use of auto-regressive base models to explain anomalies in terms of the underlying ODE governing the dynamics of the system under study.

- SPABC uses the concept from BAPC to break up the action of the full predictive (hybrid) model into an interpretable and a non-interpretable one. SPABC can be given any reasonably chosen base model (e.g., linear regression) modeling the bulk of the phenomena, and allowing for **parameter changes  $\Delta f_r$  to explain the correcting AI-model  $\hat{e}$** . Other surrogate models (such as LIME [23], treeSHAP[14], or windowSHAP[40]) don't use this decomposition and don't have this freedom of choice.
- The use of the descriptive power of models with physical parameters (such as (4)) can be used via relations to purely data driven discrete time models (such as Prop. 1-3) for which the definition of SBAPC fits without introducing a discretization error.
- SBAPC highlights the feature importance by the help of the integrated gradient concept which helps to break up the corresponding contributions in the specific features cumulative way over the time period of the considered windows. A heatmap (Fig. 10) shows the ranges in which the explanations are strongest.
- The correction window size ( $r$ ) represents the key parameter of the local surrogate approach. Our experiments (see Sect. 5.3) show that for typical change points there is a maximum in the strength of the explanation  $\Delta f_r$ . This coincides with observations about such a maximum made if linear regression is chosen as the base model [31].
- There is no weighted sub-sampling method as used in LIME. Instead, a specific window size parameter  $r$  is singled out which is characteristic of the explanation being strongest (maximal  $|\Delta f_r|$ ). This shows that the BAPC-concept allows an automatic parameter-choice of the local surrogate modeling overcoming LIME's lack of determination [19] in the size of the neighborhood. **SBAPC's unique interpretation is that of the most expressive explanation.**



Currently, we are working on applying this method to several other industrial use cases and their challenges related to explainability in AI-driven corrections addressing changes in physical systems.

We believe SBAPC to be a powerful contribution in the field of model agnostic local surrogate explainability of predictive time series learning models. We also believe that this will play an important role in the ongoing competition between the different local surrogate approaches to explainable AI by overcoming LIME’s instability problem [39].

## Acknowledgement

This work has been supported by the project ‘inAIco’ (FFG-Project No. 862019; Bridge Young Scientist, 2020), the BMK, BMAW, the #upperVision2030 project SPA, and the State of Upper Austria in the frame of the SCCH competence center INTEGRATE [(FFG grant no. 892418)] as part of the FFG COMET Competence Centers for Excellent Technologies Programme.

## Disclosure

The authors have no competing interests to declare that are relevant to the content of this article.

## A Appendix

### A.1 Proofs of Propositions

In this section, we provide proofs of our propositions and establish some technical lemmas.

*Proof of Proposition 1.* It is clear that  $y_1 = \alpha \cos(\phi)$  and  $y_2 = \alpha \exp(-\beta) \cos(\omega + \phi)$ . Let us take  $z = -\beta + i\omega$  and  $t \in \{3, \dots, n\}$ . We have

$$\begin{aligned} \exp(zt) &= \exp(z(t-1)) \exp(z) + \exp(z(t-1)) \exp(-z-2\beta) - \exp(-2\beta) \exp(z(t-2)) \\ &= \exp(z(t-1))(\exp(z) + \exp(\bar{z})) - \exp(-2\beta) \exp(z(t-2)) \\ &= \exp(z(t-1))2 \exp(-\beta) \cos(\omega) - \exp(-2\beta) \exp(z(t-2)) \\ &= \varphi_1 \exp(z(t-1)) + \varphi_2 \exp(z(t-2)). \end{aligned}$$

Then we obtain that

$$\begin{aligned} y_{t+1} &= \operatorname{Re}\{\alpha \exp(i\phi) \exp(zt)\} \\ &= \operatorname{Re}\{\alpha \exp(i\phi)(\varphi_1 \exp(z(t-1)) + \varphi_2 \exp(z(t-2)))\} \\ &= \varphi_1 \operatorname{Re}\{\alpha \exp(i\phi) \exp(z(t-1))\} + \varphi_2 \operatorname{Re}\{\alpha \exp(i\phi) \exp(z(t-2))\} \\ &= \varphi_1 y_{t-1} + \varphi_2 y_{t-2} \end{aligned}$$

and so the result is proved.  $\square$

*Proof of Proposition 2.* let us denote  $y(t) = \operatorname{Re}\{\alpha \exp(i\phi) \exp(zt)\}$ , with  $z = -\beta + i\omega$ . We have  $y(0) = \operatorname{Re}\{\alpha \exp(i\phi)\} = \alpha \cos \phi = y_1$  and

$$\begin{aligned} y(1) &= \operatorname{Re}\{\alpha \exp(i\phi) \exp(z)\} = \alpha \exp(-\beta) \cos(\omega + \phi) \\ &= \alpha \exp(-\beta) \cos \omega \cos \phi - \alpha \exp(-\beta) \sin \omega \sin \phi \\ &= y_1 \exp(-\beta) \cos \omega - y_1 \exp(-\beta) \sin \omega \tan \phi = y_2. \end{aligned}$$

Let us show now that  $y_t = y(t-1)$ ,  $t = 3, \dots, n$ , by induction on  $t$ . Given that  $\varphi_1 = 2 \exp(-\beta) \cos(\omega)$  and  $\varphi_2 = -\exp(-2\beta)$ , we obtain

$$\begin{aligned} \varphi_1 \exp(z) + \varphi_2 &= 2 \exp(-\beta) \cos(\omega) \exp(z) - \exp(-2\beta) \\ &= (\exp(z) + \exp(\bar{z})) \exp(z) - \exp(-2\beta) \\ &= \exp(2z) + \exp(z + \bar{z}) - \exp(-2\beta) = \exp(2z). \end{aligned}$$

Therefore

$$y_3 = \varphi_1 y_2 + \varphi_2 y_1 = \operatorname{Re}\{\alpha \exp(i\phi) (\varphi_1 \exp(z) + \varphi_2)\} = \operatorname{Re}\{\alpha \exp(i\phi) \exp(2z)\} = y(2).$$

Assuming that  $y_k = y(k-1)$  for  $k = 1, \dots, t$ , we obtain

$$\begin{aligned} \varphi_1 \exp(z(t-1)) + \varphi_2 \exp(z(t-2)) &= \exp(z(t-2)) (\varphi_1 \exp(z) + \varphi_2) \\ &= \exp(z(t-2)) \exp(2z) = \exp(zt), \end{aligned}$$

and so

$$\begin{aligned} y_{t+1} &= \varphi_1 y_t + \varphi_2 y_{t-1} = \varphi_1 y(t-1) + \varphi_2 y(t-2) \\ &= \operatorname{Re}\{\alpha \exp(i\phi) (\varphi_1 \exp(z(t-1)) + \varphi_2 \exp(z(t-2)))\} \\ &= \operatorname{Re}\{\alpha \exp(i\phi) \exp(zt)\} = y(t), \end{aligned}$$

which concludes the proof.  $\square$

**Lemma 1.** Let  $f : \mathbb{R} \times \mathbb{R}^n \rightarrow \mathbb{R}$  be defined as  $f(x, y) = x \exp(\mu^\top y)$  with  $\mu \in \mathbb{C}^n$ . Then for any  $x, \Delta x \in \mathbb{R}$  and  $y, \Delta y \in \mathbb{R}^n$ , it holds that

$$\Delta x \int_0^1 \frac{\partial f}{\partial x}(x + h\Delta x, y + h\Delta y) dh = \Delta x \frac{\Delta g}{\mu^\top \Delta y} \quad (16)$$

$$\Delta y_k \int_0^1 \frac{\partial f}{\partial y_k}(x + h\Delta x, y + h\Delta y) dh = \frac{\mu_k \Delta y_k}{\mu^\top \Delta y} \left( \Delta f - \Delta x \frac{\Delta g}{\mu^\top \Delta y} \right), \quad (17)$$

for every  $k = 1, \dots, n$ , where  $\Delta g := \exp(\mu^\top (y + \Delta y)) - \exp(\mu^\top y)$  and  $\Delta f := f(x + \Delta x, y + \Delta y) - f(x, y)$ .

*Proof.* Denoting by  $I$  the left-hand side of (16), we have

$$I = \Delta x \int_0^1 \exp(\mu^\top (y + h\Delta y)) dh = \frac{\Delta x}{\mu^\top \Delta y} \exp(\mu^\top (y + h\Delta y)) \Big|_0^1 = \Delta x \frac{\Delta g}{\mu^\top \Delta y}.$$

Let us now denote by  $J$  the left-hand side of (17). Integrating by part we obtain

$$\begin{aligned}
J &= \Delta y_k \mu_k \int_0^1 (x + h\Delta x) \exp(\mu^\top(y + h\Delta y)) dh \\
&= \frac{\Delta y_k \mu_k}{\mu^\top \Delta y} \left( (x + h\Delta x) \exp(\mu^\top(y + h\Delta y)) \Big|_0^1 - \Delta x \int_0^1 \exp(\mu^\top(y + h\Delta y)) dh \right) \\
&= \frac{\Delta y_k \mu_k}{\mu^\top \Delta y} \left( (x + h\Delta x) \exp(\mu^\top(y + h\Delta y)) \Big|_0^1 - \frac{\Delta x}{\mu^\top \Delta y} \exp(\mu^\top(y + h\Delta y)) \Big|_0^1 \right)
\end{aligned}$$

which implies (17).  $\square$

*Proof of Proposition 5-(iii).* For  $t = 0, 1$  the function  $\boldsymbol{\theta} \mapsto f_\theta(t)$  is constant, therefore  $\text{IG}_1(f_\theta, 0) = \text{IG}_1(f_\theta, 1) = \text{IG}_2(f_\theta, 0) = \text{IG}_2(f_\theta, 1) = 0$ . Let us now show the result for  $t = 3, \dots, n$ . Given  $a, b, c, d \in \mathbb{R}$  and  $m, n \in \mathbb{Z}_+$ , using the binomial formula it follows that

$$\int_0^1 \gamma^m(a, b, h) \gamma^n(c, d, h) dh = \sum_{j=0}^m \sum_{k=0}^n \binom{m}{j} \binom{n}{k} \frac{a^{m-j} (b-a)^j c^{n-k} (d-c)^k}{j+k+1}. \quad (18)$$

Denoting  $\gamma(h) := \gamma(\boldsymbol{\varphi}_r, \boldsymbol{\varphi}_0, h)$ , we obtain from (6) that

$$\frac{\partial \Phi}{\partial \varphi_1}(t, \gamma(h)) = \sum_{k=0}^{\lfloor t/2 \rfloor} \binom{t-k}{k} (t-2k) \gamma_1^{t-1-2k}(h) \gamma_2^k(h), \quad (19)$$

and so (18) implies,

$$\int_0^1 \frac{\partial \Phi}{\partial \varphi_1}(t, \gamma(h)) dh = \bar{\Phi}_1(t, 0). \quad (20)$$

Recall that  $\Phi_1(t, \boldsymbol{\varphi}) = \Phi(t-2, \boldsymbol{\varphi})$  by definition, so from (20) it follows that

$$\int_0^1 \frac{\partial \Phi_1}{\partial \varphi_1}(t, \gamma(h)) dh = \bar{\Phi}_1(t-2, 0) \quad (21)$$

Similarly, given that  $\Phi_2(t, \boldsymbol{\varphi}) = \varphi_2 \Phi(t-3, \boldsymbol{\varphi})$ , it follows from (19) that

$$\begin{aligned}
\frac{\partial \Phi_2}{\partial \varphi_1}(t+3, \gamma(h)) &= (\varphi_{r2} + h\Delta\varphi_{2r}) \frac{\partial \Phi}{\partial \varphi_1}(t, \gamma(h)) \\
&= \sum_{k=0}^{\lfloor t/2 \rfloor} \binom{t-k}{k} (t-2k) \gamma^{t-1-2k}(h) \gamma^{k+1}(h)
\end{aligned}$$

and so

$$\int_0^1 \frac{\partial \Phi_2}{\partial \varphi_1}(t, \gamma(h)) dh = \bar{\Phi}_1(t-3, 1) \quad (22)$$

Therefore, from (21) and (22), we obtain (12). The proof of (13) follows from similar arguments.  $\square$

## A.2 ODE governed time-series

The time series displayed at the first row of Figure 3 and at Figure 4a correspond to discrete observations of the form

$$y_t = u(t - 1), \quad t = 1, \dots, n$$

where  $u : \mathbb{R} \rightarrow \mathbb{R}$  is the solution of a non-homogeneous initial value problem (IVP), or one with time-dependent coefficients; see Table 3 and Proposition 6.

Table 3: Synthetic data description.

Data	$u(t)$	$u_0$	$v_0$	Param.	$t^*$
Step	$u_0 + FH(t - t^*)$	-1	-	$F = 2$	48.5
Ramp	$u_0 + v_0 t + FH(t - t^*)$	23.5	-1	$F = 2$	48.5
SinACP	$u_0 \cos(\omega t) + H(t - t^*)(F/w) \sin(\omega(t - t^*))$	1	0	$\omega = 2\pi/24$ $F = -\omega$	55
SinFCP	$\begin{cases} u_0 \cos(\omega t) & \text{if } t < t^* \\ u_0 \cos(\nu t + (\omega - \nu)t^*) & \text{if } t \geq t^* \end{cases}$	1	0	$\omega = 2\pi/40$ $\nu = 2\omega$	81

These data represent discrete observations of the one-dimensional position of an object (or another one-dimensional dynamical system) governed by an ordinary differential equation (ODE). In the cases of Step, Ramp, and SinACP, these observations correspond to scenarios where an external force  $F \in \mathbb{R}$  acts at a specific time  $t^* \in \mathbb{R}$  for a very short duration, causing a significant change in the object's position or velocity [38]. Mathematically, such external forces are modeled as  $F\delta(\cdot - t^*)$ , where  $\delta$  denotes the Dirac delta distribution.

Examples of such scenarios include hitting a nail with a hammer (Step), kicking an oncoming football in the opposite direction (Ramp), and a mass attached to a string subjected to an impulsive external force (SinACP). In the case of SinFCP, the observed data correspond to a situation where a mass attached to a string undergoes a sudden loss of mass and/or an increase in string stiffness.

In what follows, we show that the functions  $u$  in Table 3 are solutions to specific IVP formulated within the framework of distribution theory. For a detailed theoretical background on the distribution theory applied in this paper, we refer the reader to [8].

**Lemma 2.** *Let  $\mathcal{F}$  be the Fourier transform over distributions,  $H$  the Heaviside function on the real line and  $\omega > 0$ , then we have the formulas:*

1.  $\mathcal{F}\{\sin(\omega \cdot)\}(\xi) = -i\pi(\delta(\xi - \omega) - \delta(\xi + \omega))$
2.  $\mathcal{F}\{\cos(\omega \cdot)\}(\xi) = \pi(\delta(\xi - \omega) + \delta(\xi + \omega))$
3.  $\mathcal{F}\{H \sin(\omega \cdot)\}(\xi) = \frac{1}{2} \mathcal{F}\{\sin(\omega \cdot)\}(\xi) + \frac{\omega}{\omega^2 - \xi^2}$
4.  $\mathcal{F}\{H \cos(\omega \cdot)\}(\xi) = \frac{1}{2} \mathcal{F}\{\cos(\omega \cdot)\}(\xi) + \frac{i\xi}{\omega^2 - \xi^2}$

*Proof.* These formulas are well known, see for instance [36].  $\square$

**Lemma 3.** *Given  $\omega > 0$  we have*

1.  $|t|'' = 2\delta(t)$
2.  $(H(t) \sin(\omega t))'' = H(t)\omega^2 \sin(\omega t) - \omega\delta(t)$
3.  $(H(t) \cos(\omega t))'' = H(t)\omega^2 \cos(\omega t) - \delta'(t)$

*Proof.*

1. See Problem 4.1 in [8].
2. This result is proved in Problem 9.14 in [8], here we provide an alternative proof. Recall that for a given distribution  $v$  it holds that

$$v''(t) = \mathcal{F}^{-1} \{ \xi^2 \mathcal{F} \{ v \} (\xi) \}. \quad (23)$$

Now, from Lemma 2 part 3, we have

$$\xi^2 \mathcal{F} \{ H \sin(\omega \cdot) \} (\xi) = \xi^2 \frac{1}{2} \mathcal{F} \{ \sin(\omega \cdot) \} (\xi) + \frac{\xi^2 \omega}{\omega^2 - \xi^2}. \quad (24)$$

Therefore, from (23) and (24) we obtain

$$(H(t) \sin(\omega t))'' = \frac{1}{2} \omega^2 \sin(\omega t) + \mathcal{F}^{-1} \left\{ \frac{\xi^2 \omega}{\omega^2 - \xi^2} \right\} (t). \quad (25)$$

Also, it can be shown that

$$\mathcal{F}^{-1} \left\{ \frac{\xi^2 \omega}{\omega^2 - \xi^2} \right\} (t) = \frac{1}{2} \operatorname{sgn}(t) \omega^2 \sin(\omega t) - \omega \delta(t), \quad (26)$$

and so the result follows by combining (25) and (26).

3. The result is obtained by following the steps of the part 2 and proceeding analogously. Instead of (26) we now use the formula

$$\mathcal{F}^{-1} \left\{ \frac{i\xi^3}{\omega^2 - \xi^2} \right\} (t) = \frac{1}{2} \operatorname{sgn}(t) \omega^2 \cos(\omega t) - \delta'(t).$$

$\square$

**Proposition 6.** *For  $u_0, v_0, F \in \mathbb{R}$  and  $t^*, \omega, \nu > 0$ , we have the following initial value problems (IVP) solutions:*

1. *The distribution*

$$u(t) = u_0 + FH(t - t^*), \quad (27)$$

*is solution of the IVP  $u'(t) = F\delta(t - t^*)$ ,  $u(0) = u_0$ , where  $H$  denotes the Heaviside function.*

2. The distribution

$$u(t) = u_0 + v_0 t + FH(t - t^*), \quad (28)$$

is solution of the IVP  $u''(t) = F\delta(t - t^*)$ ,  $u(0) = u_0$ ,  $u'(0) = v_0$ .

3. The distribution

$$u(t) = u_0 \cos(\omega t) + H(t - t^*)(F/\omega) \sin(\omega(t - t^*)), \quad (29)$$

is solution of the IVP  $u''(t) + \omega^2 u(t) = F\delta(t - t^*)$ ,  $u(0) = u_0$ ,  $u'(0) = 0$ .

4. The distribution

$$u(t) = \begin{cases} u_0 \cos(\omega t) & \text{if } t \leq t^* \\ u_0 \cos(\nu t + (\omega - \nu)t^*) & \text{if } t > t^* \end{cases} \quad (30)$$

is solution of the IVP  $u''(t) + (\omega^2 + H(t - t^*)(\nu^2 - \omega^2))u(t) = 0$ ,  $u(0) = u_0$ ,  $u'(0) = 0$ .

*Proof.*

1. It is a direct consequence from the fact that  $u_h := u_0$  satisfies the homogeneous equation and that  $H' = \delta$  (see for instance Example 4.2 in [8]).
2. We have that the distribution  $u_0 + v_0 t + F/2 (t - t^*)$  satisfies the homogeneous equation and that  $|\cdot|'' = 2\delta$  (see Lemma 3 part 1), which implies the result.
3. It is easy to check that  $u_h = u_0 \cos(\omega t)$  is a solution of the homogeneous equation. Also, from Lemma 3 part 2, it follows that the distribution  $u_p := H(t)(F/\omega) \sin(\omega(t))$  satisfies  $u_p'' + \omega^2 u_p = F\delta$ . Therefore  $u = u_h + u_p(t - t^*)$  satisfies the IVP.
4. For simplicity, let us prove the result for  $t^* = 0$  and  $u_0 = 1$ , the general case follows from analogous argument. In this case,  $u(t) = \cos(\omega t) - H(t) \cos(\omega t) + H(t) \cos(\nu t)$  and so the result follows from Lemma 3 part 3.

□

## References

- [1] Anonymous. “Toward Physics-guided Time Series Embedding”. In: *Submitted to The Thirteenth International Conference on Learning Representations*. under review. 2024. URL: <https://openreview.net/forum?id=rJ1xGcJVu8>.
- [2] Ivo Bukovsky, Witold Kinsner, and Noriyasu Homma. “Learning Entropy as a Learning-Based Information Concept”. In: *Entropy* 21.2 (2019), p. 166.

- [3] Nadja Burkart and Marco F. Huber. “A Survey on the Explainability of Supervised Machine Learning”. In: *arXive* (2020). (see discussion in the introduction). URL: <https://doi.org/10.48550/arXiv.2011.07876>.
- [4] Diogo V Carvalho, Eduardo M Pereira, and Jaime S Cardoso. “Machine learning interpretability: A survey on methods and metrics”. In: *Electronics* 8.8 (2019), p. 832.
- [5] Jorge A Chan-Lau et al. “Surrogate Data Models: Interpreting Large-scale Machine Learning Crisis Prediction Models”. In: *IMF Working Papers* 2023.041 (2023), A001.
- [6] R.N. Chaudhuri. *Waves and Oscillations*. Basic physics through problems series. New Age International, 2001. ISBN: 9788122412918. URL: <https://books.google.at/books?id=o-ythNqfmA8C>.
- [7] Filip Karlo Došilović, Mario Brčić, and Nikica Hlupić. “Explainable artificial intelligence: A survey”. In: *2018 41st International convention on information and communication technology, electronics and microelectronics (MIPRO)*. IEEE. 2018, pp. 0210–0215.
- [8] Johannes Jisse Duistermaat and Johan A.C. Kolk. *Distributions: Theory and Applications*. Basel: Birkhäuser, 2010. DOI: 10.1007/978-3-7643-8742-2. URL: <https://doi.org/10.1007/978-3-7643-8742-2>.
- [9] Fabian Fumagalli et al. “KernelSHAP-IQ: Weighted Least Square Optimization for Shapley Interactions”. In: *arXive* (2024). URL: <https://doi.org/10.48550/arXiv.2405.10852>.
- [10] D Gunning. “Explainable artificial intelligence (xai) darpa-baa-16-53”. In: *Defense Advanced Research Projects Agency* (2016).
- [11] Sepp Hochreiter and Jürgen Schmidhuber. “Long Short-Term Memory”. In: *Neural Computation* 9.8 (1997), pp. 1735–1780.
- [12] *Agnostic local explanation for time series classification*. 2019, pp. 432–439.
- [13] John Konvalina. “A Combinatorial Formula for Powers of  $2 \times 2$  Matrices”. In: *Mathematics Magazine* 88.4 (2015), pp. 280–284. DOI: 10.4169/math.mag.88.4.280.
- [14] S.M. Lundberg, G. Erion, and H. Chen. “From local explanations to global understanding with explainable AI for trees”. In: *Nat Mach Intell* 2 (2020), pp. 56–67.
- [15] Daniel Lundstrom, Tianjian Huang, and Meisam Razaviyayn. “A Rigorous Study of Integrated Gradients Method and Extensions to Internal Neuron Attributions”. In: *ArXiv abs/2202.11912* (2022). URL: <https://api.semanticscholar.org/CorpusID:247084007>.
- [16] Helmut Lütkepohl. *New introduction to multiple time series analysis*. Springer Science & Business Media, 2005.

- [17] Han Meng, Christian Wagner, and Isaac Triguero. “SEGAL time series classification — Stable explanations using a generative model and an adaptive weighting method for LIME”. In: *Neural Networks* 176 (2024), p. 106345. ISSN: 0893-6080. DOI: <https://doi.org/10.1016/j.neunet.2024.106345>. URL: <https://www.sciencedirect.com/science/article/pii/S0893608024002697>.
- [18] D. Minh et al. “Explainable artificial intelligence: a comprehensive review”. In: *Artif Intell Rev* 55 (2022), pp. 3503–3568.
- [19] Christoph Molnar. *Interpretable Machine Learning – A Brief History, State-of-the-Art and Challenges*. ebook, 2019. URL: <https://christophm.github.io/interpretable-ml-book/>.
- [20] Simon Neugebauer et al. “Explainability of AI-predictions based on psychological profiling”. In: *Procedia Computer Science* 180 (2021). Proceedings of the 2nd International Conference on Industry 4.0 and Smart Manufacturing (ISM 2020), pp. 1003–1012. ISSN: 1877-0509. DOI: <https://doi.org/10.1016/j.procs.2021.01.361>. URL: <https://www.sciencedirect.com/science/article/pii/S1877050921004385>.
- [21] Simon Neugebauer et al. “Explainability of AI-predictions based on psychological profiling”. In: *Procedia Computer Science* 180 (2021). Proceedings of the 2nd International Conference on Industry 4.0 and Smart Manufacturing (ISM 2020), pp. 1003–1012.
- [22] Ozan Ozyegen, Igor Ilic, and Mucahit Cevik. “Evaluation of interpretability methods for multivariate time series forecasting”. In: *Appl. Intell.* 52.5 (2022), pp. 4727–4743.
- [23] Marco Tulio Ribeiro, Sameer Singh, and Carlos Guestrin. ““Why Should I Trust You?”: Explaining the Predictions of Any Classifier”. In: *Proceedings of the 22nd ACM SIGKDD International Conference on Knowledge Discovery and Data Mining, KDD '16*. New York, NY, USA: Association for Computing Machinery, 2016, pp. 1135–1144. ISBN: 9781450342322.
- [24] Thomas Rojat et al. “Explainable artificial intelligence (xai) on timeseries data: A survey”. In: *arXiv preprint arXiv:2104.00950* (2021).
- [25] Waddah Saeed and Christian Omlin. “Explainable AI (XAI): A systematic meta-survey of current challenges and future opportunities”. In: *Knowledge-Based Systems* 263 (2023), p. 110273.
- [26] Rohit Saluja et al. *Towards a Rigorous Evaluation of Explainability for Multivariate Time Series*. 2021. arXiv: 2104.04075 [cs.LG].
- [27] Udo Schlegel et al. “TS-MULE: Local Interpretable Model-Agnostic Explanations for Time Series Forecast Models”. In: *Machine Learning and Principles and Practice of Knowledge Discovery in Databases*. Cham: Springer International Publishing, 2021, pp. 5–14. ISBN: 978-3-030-93736-2.
- [28] Udo Schlegel et al. *TS-MULE: Local Interpretable Model-Agnostic Explanations for Time Series Forecast Models*. 2021. arXiv: 2109.08438 [cs.LG].



- [29] Kaan Sel et al. “Physics-informed neural networks for modeling physiological time series for cuffless blood pressure estimation”. In: *npj Digit. Medicine* 6 (2023).
- [30] Torty Sivill and Peter Flach. “LIMESegment: Meaningful, Realistic Time Series Explanations”. In: *Proceedings of The 25th International Conference on Artificial Intelligence and Statistics*. Ed. by Gustau Camps-Valls, Francisco J. R. Ruiz, and Isabel Valera. Vol. 151. Proceedings of Machine Learning Research. PMLR, 2022, pp. 3418–3433. URL: <https://proceedings.mlr.press/v151/sivill22a.html>.
- [31] Florian Sobieczky and Manuela Geiß. “Explainable AI by BAPC – Before and After correction Parameter Comparison”. In: *arXiv:2103.07155* (2023).
- [32] Erik Štrumbelj and Igor Kononenko. “Explaining prediction models and individual predictions with feature contributions”. In: *Knowledge and Information Systems* 41 (2014), pp. 647–665.
- [33] Mukund Sundararajan and Amir Najmi. “The Many Shapley Values for Model Explanation”. In: *Proceedings of the 37th International Conference on Machine Learning*. Ed. by Hal Daumé III and Aarti Singh. Vol. 119. Proceedings of Machine Learning Research. PMLR, 2020, pp. 9269–9278.
- [34] Mukund Sundararajan, Ankur Taly, and Qiqi Yan. “Axiomatic attribution for deep networks”. In: *International conference on machine learning*. PMLR. 2017, pp. 3319–3328.
- [35] R Core Team. *R Package: datasets*. R package version 4.4.1. 2024. URL: <https://CRAN.R-project.org/package=datasets>.
- [36] The Fourier Transform Team. *The Fourier Transform*. Accessed: 2024-12-27. 2024. URL: <https://www.thefouriertransform.com/>.
- [37] Andreas Theissler et al. “Explainable AI for Time Series Classification: A Review, Taxonomy and Research Directions”. In: *IEEE Access* 10 (2022), pp. 100700–100724. DOI: 10.1109/ACCESS.2022.3207765.
- [38] Brooks Thomas. *Slightly Disturbed: A Mathematical Approach to Oscillations and Waves*. 2017.
- [39] Giorgio Visani, Enrico Bagli, and Federico Chesani. “OptiLIME: Optimized LIME Explanations for Diagnostic Computer Algorithms”. In: *arXiv* (2020). URL: <https://doi.org/10.48550/arXiv.2006.05714>.
- [40] “WindowSHAP: An efficient framework for explaining time-series classifiers based on Shapley values”. In: *Journal of Biomedical Informatics* 144 (2023), p. 104438. ISSN: 1532-0464. DOI: <https://doi.org/10.1016/j.jbi.2023.104438>. URL: <https://www.sciencedirect.com/science/article/pii/S1532046423001594>.
- [41] Xiubin Zhu et al. “Fuzzy Rule-Based Local Surrogate Models for Black-Box Model Explanation”. In: *IEEE Transactions on Fuzzy Systems* 31.6 (2023), pp. 2056–2064. DOI: 10.1109/TFUZZ.2022.3218426.